Obtaining population indices from video observations of meteors

Sirko Molau[1], **Geert Barentsen**[2], **and Stefano Crivello**[3]

[1]**Abenstalstr. 13b, 84072 Seysdorf, Germany**
sirko@molau.de

[2]**University of Hertfordshire, College Lane, Hatfield, AL10 9AB, U.K.**
geert@barentsen.be

[3]**Via Bobbio 9a/18, 16137 Genova, Italy**
stefano.crivello@libero.it

We present a novel approach for the determination of the population index from meteor showers, which is particularly useful for video camera networks with a large range of limiting magnitudes. Unlike previous approaches in the visual domain, it compares the meteor counts from cameras with different limiting magnitudes to derive the population index. Thus, it is totally independent of the meteor brightness estimate and also resistant to systematic errors in the limiting magnitude calculation or the detection efficiency close to the limiting magnitude of a camera. We derive the new approach step-by-step and present a number or refinements to improve the basic algorithm. Using the Poisson distribution gives the approach a solid probabilistic base and weights each data set according to its contribution to the population index. Finally we present and discuss first preliminary population index profiles obtained from the IMO Video Meteor Network.

1 Introduction

The population index or *r*-value describes the brightness distribution in a meteor shower, or more specifically by what factor the total number of shower meteors increases when the limiting magnitude improves by one magnitude.

As Rendtel (2013) pointed out, the population index plays a vital role in the determination of zenithal hourly rates *ZHRs*, equation (1) and flux densities *FD*, equation (2) from visual and video observations.

$$ZHR = \frac{MC * r^{6.5-LM} * F}{T_{eff} * (\cos ZD)^{\gamma}} \qquad (1)$$

$$FD = \frac{MC * r^{6.5-LM}}{T_{eff} * (\cos ZD)^{\gamma} * CA} \qquad (2)$$

Both equations (1) and (2) look fairly similar, because they are proportional to one another and express the same quantity (meteor shower activity) under different boundary conditions. The *ZHR* is normalized to the "average human field of view", whereas the flux density refers to a standardized collection area in the atmosphere. Identical ingredients are the meteor count *MC*, limiting magnitude *LM*, zenith distance of the radiant *ZD* and the zenith exponent γ. Visual observations are additionally corrected by a factor *F* that describes the obstruction of the field of view, whereas video observations are normalized by the collection area *CA* of the camera.

The impact of the population index *r* is apparent. When *LM* is 6.5, the population index term becomes unity. However, the bigger the difference between the actual limiting magnitude and the reference value of 6.5 mag, the larger becomes the impact of *r*. This is particularly true for video observations. Whereas visual observers often report limiting magnitudes around 6, the *LM* of many video cameras is in the range of magnitude 3 to 4.

To give an example: when the unexpected outburst of the September Perseids (SPE) in 2013 was analyzed first, we used a population index of *r=3.0* as there were no other data available, and obtained a remarkable peak flux density of 70 meteoroids per 1000 km^2 and hour. Later we found that the population index was exceptionally low with *r=1.4*, which reduced the peak flux to 2 (Rendtel et al., 2014).

2 Current state

Up to now, all flux densities obtained from data of the IMO Video Meteor Network (Molau and Barentsen, 2013) were derived with a fixed shower-specific population index taken from the IMO Working List of Meteor Showers. The data originate from earlier analyses of visual observations, and any variation of *r* over time was ignored.

There are two methods to derive population indexes from visual data, and both are based on the meteor brightness distribution. One compares the cumulative meteor counts for different meteor brightness classes well below the limiting magnitude (to account for the fact that the human detection probability for meteors degrades significantly close to the limiting magnitude). The other one relates the average meteor brightness to the limiting magnitude, and gives more robust estimates (Arlt, 2003). In any case, certain prerequisites have to be met for these procedures to work:

- There should be no systematic error in the brightness estimation of meteors.
- The detection probability of meteors should be known as a function of their brightness.
- There should be no systematic error in the limiting magnitude estimation.

Let us compare these prerequisites with the characteristics of video observation obtained by the IMO Video Meteor Network:

- Contrary to other video networks with standardized equipment, there is a large variety of cameras with a wide range of fields of view and limiting magnitudes.
- Brightness estimates of meteors obtained by MetRec are unreliable, because the measurement of faint objects in noisy video frames is challenging.
- The effective observing time, field of view and limiting magnitude of each camera are precisely known.
- The detection probability for meteors depends neither on where in the field of view nor when a meteor is observed. The only relevant factors are the meteor brightness and angular velocity.

The lack in meteor brightness accuracy makes the visual standard procedures for population index calculation unsuitable. So why not take advantage of the disadvantage, that the cameras in the IMO network cover such a wide range of properties?

It is a well-known fact that wide-angle cameras with low limiting magnitude perform best when there are many bright meteors, whereas cameras with smaller fields of view and better limiting magnitude act best, when the population index is high and there are many faint meteors. More precisely, there is a direct dependency of the meteor detection ratio between wide and narrow angle cameras and the population index.

3 A new approach for calculating population indices

As described earlier, the flux density of each camera is currently calculated for a typical *r*-value only. The basic idea of the new approach is that the flux density is calculated for each camera and for each possible population index. Then the population index is chosen such that the individual flux densities of all cameras agree best with one another. By this approach we get directly both the optimal population index and flux density.

Since the calculation of the flux density is time-consuming, it would be welcome if the dependency from the population index would be mathematically simple, e.g. linear. Unfortunately that is not the case. Equation (3) is a refinement of equation (2) to cover specific aspects of flux density calculation of meteor showers:

$$FD = \frac{MC}{T_{eff} * (\cos ZD)^{\gamma} * \sum_{pix} \frac{CA}{r^{6.5-MLM}}} \qquad (3)$$

Most notably, the (stellar) limiting magnitude *LM* is replaced here by the meteor limiting magnitude *MLM*. Equation (3) contains terms which are fixed over the field of view (meteor count, effective observing time, radiant zenith distance and zenith exponent) and terms which vary from pixel to pixel. These are in particular the collection area and the meteor limiting magnitude. The angular velocity of a meteor depends on the radiant distance and altitude. At a pixel which is farther away from the radiant and higher in the sky, the meteor is apparently moving faster, the photons are spread over more pixels and thus the meteor limiting magnitude will reduce more. For this reason, the collection area and limiting magnitude correction are summed up over all pixels which lead to a complex dependency of *FD* from *r*. In order to reduce the computational overhead we shall find a suitable approximation for this dependency (Figure1).

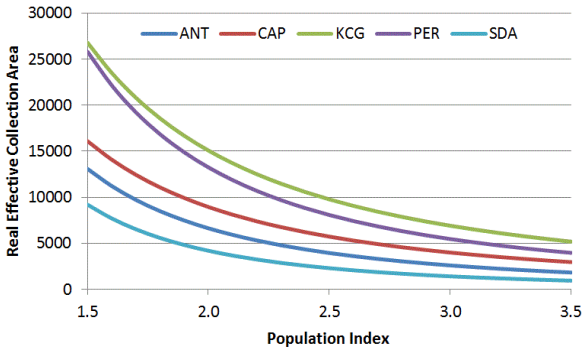

Figure 1 – Dependency of the flux density (which is inversely proportional to the effective collection area) from the population index, calculated for a particular non-intensified video camera in mid-August 2013.

A first approximation is to replace the variable meteor limiting magnitude *MLM* by the average value *AVGMLM*, equation (4), over all pixels. Thus we can pull the term with the population index out of the pixel sum.

$$FD \approx \frac{MC * r^{6.5-AVGMLM}}{T_{eff} * (\cos ZD)^{\gamma} * \sum_{pix} CA} \qquad (4)$$

However, tests with real observational data from August 2013 have shown that this will introduce significant approximation errors of up to 50% relative when a large range of population indexes shall be covered (Figure 2).

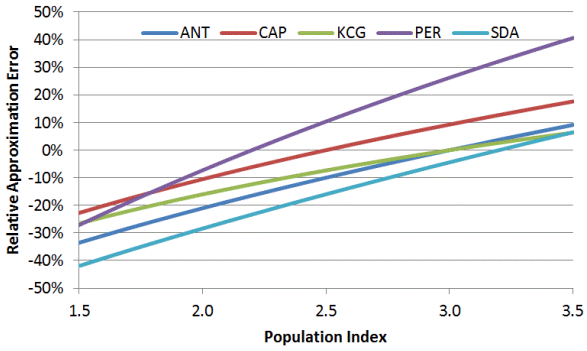

Figure 2 – Approximation error when the limiting meteor magnitude per pixel *MLM* is replaced by the average limiting magnitude *AVGMLM*. If the population index deviates significantly from the shower-specific start value, the relative error may become as big as 50% (same data set as Figure 1).

More promising is another approach to calculate the flux density for small set of selected *r*-values (e.g. between 1.5 and 3.5 in steps of 0.1) and then fit a parametric function that approximates the dependency of *FD* from *r*. Since in the flux density equations the population index *r* is always taken to the power of some magnitude value it is no surprise that a power function of type $a * r^b$ yields a good approximation. In fact, this approach is a refined version of the first approximation whereby the power exponent is not calculated as the mean meteor limiting magnitude over the full field of view, but estimated from data. Even when a wide range of *r*-values is selected, the relative error is always below 3% (Figure 3). When the parameters *a* and *b* of the power function are not calculated once for the full night, but individually for every observing minute, the approximation error is halved once more (Figure 4).

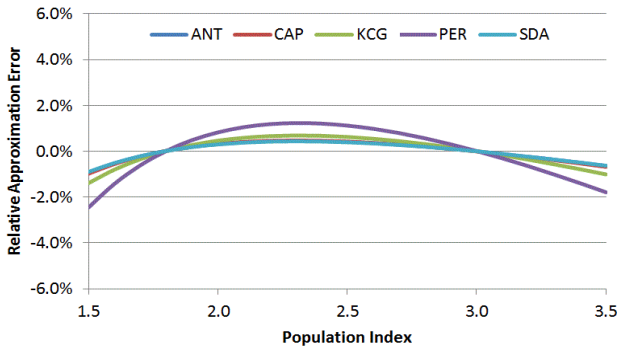

Figure 3 – Approximation error, when a power function of type $a * r^b$ is fitted to the dependency of the flux density from the population index over the full night. The relative error is always lower than 3% (same data set as Figure 2).

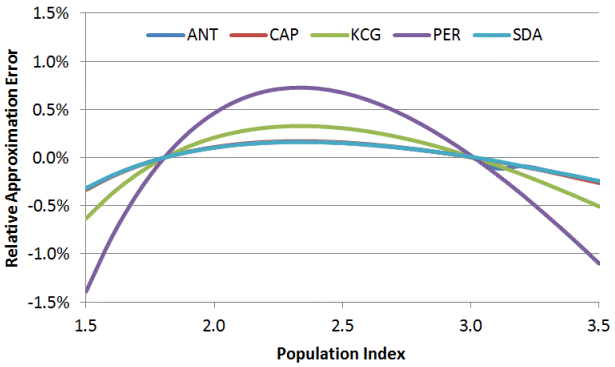

Figure 4 – Same data set as Figure 3, but the power function is fitted every minute. The approximation error has once more decreased by a factor of 2 and is now well within the error margins of other assumptions and approximations in the population index calculation.

In summary, we approximate the complex non-linear dependency of *FD* from *r* by a power function of type $a * r^b$ whose parameters are calculated and stored for every observing minute.

Initially we calculate the flux density with some predefined population index r_{start}. When we want to obtain the flux density for another population index, r_{new}, we only have to multiply it with the correction factor $CF = r_{start}^{\ b} / r_{new}^{\ b}$.

So the scaling factor *a* is canceled out, and we only have to calculate and store the exponent *b* for every minute. This leads us to the following procedure for the calculation of the population index:

- For each camera and each observing minute, calculate the flux density and the power function exponent *b*, and accumulate the flux density over the full night.
- Try iteratively different *r*-values, correct the flux density for every camera and minute, and accumulate the flux density camera-wise for the full night.
- Select the population index where the flux densities of all cameras agree best.

For testing of the new procedure, we used the video data set from the unexpected September Perseids (SPE) outburst on September 9, 2013. There are no visual observations for this event, but 21 video cameras of the IMO Video Meteor Network contributed observations for that night. It was clear, that the outburst must have had a rather unusual population index, because operators of low sensitivity wide-angle cameras reported an unusual number of (bright) meteors that night, whereas more powerful intensified cameras experienced no significant increase in counts.

Figure 5 shows the result of the new procedure. Note the logarithmic presentation of the vertical axis. The closer two lines are, the smaller is the relative deviation in flux density between them.

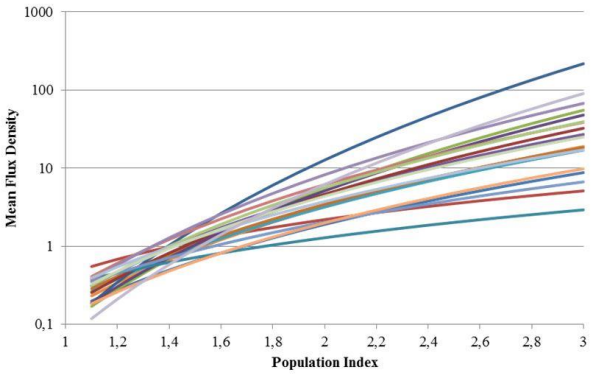

Figure 5 – Dependency of the flux density from the population index, calculated for 21 video cameras that recorded the outburst of the September Perseids on September 9, 2013. The graphs look most compact at a population index below 1.5, but the optimal value is difficult to determine.

It is clear that the procedure is working in principle and that the best population index must be somewhere close to 1.4, but it is hard to define more precisely. Cameras with limiting magnitude close to 6.5 create almost horizontal lines, and the lower the limiting magnitude of a camera, the larger is the slope. However, many cameras have similar limiting magnitudes, so their graphs are nearly parallel and will not create a well-defined point of intersection. Furthermore, even cameras with good limiting magnitude may temporarily experience clouded skies or haze, which will reduce their average *lm*.

In the next chapter we will describe a refinement to the basic approach to overcome these limitations.

4 Refinement to the basic approach

In the first approach, the data set was segmented camera-wise, because each camera has different properties. We learned, however, that the main criterion for the calculation of the population index is the meteor limiting magnitude of the camera, and that is not constant over time. It will vary in the course of a night due to twilight, moon, clouds and variable radiant distance. So a better approach is to bin the data according to this parameter. At the beginning, the limiting magnitude bins are defined, and then it is decided for each observing minute of each camera, to what bin the particular data set contributes. Figure 6 shows the result for the same SPE data set and bins of one magnitude. The result is two-fold: The number of graphs is getting smaller and the intersection angle between the graphs is increasing, which yields a more accurate intersection point.

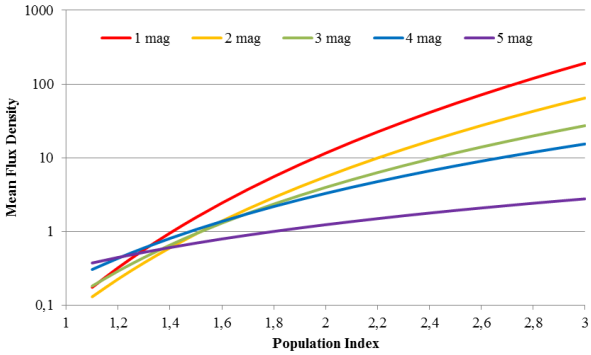

Figure 6 – Same data set as Figure 5, but now the data is not binned by camera but by the meteor limiting magnitude of each camera and observing minute.

However, the individual graphs still do not intersect exactly at one point. For this reason we now want to discuss procedures to derive the best population index under such conditions. A simple approach is to find the point where all graphs are closest to each other in a logarithmic diagram. We can visualize this by blurring the graphs and selecting the point of overall maximum intensity (Figure 7).

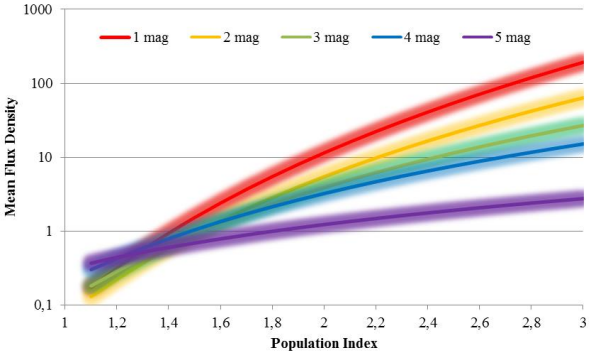

Figure 7 – Schematic plot, how the best intersection point can be determined by blurring the individual graphs and selecting the population index where the accumulated intensity is highest. Note that all graphs have the same weight in this approach.

The drawback for this procedure is that it gives all graphs the same weight, no matter how much data they contain and how discriminant they are for the population index calculation. This is avoided by a data-driven definition of the limiting magnitude bins. Instead of giving each bin the same size of one mag, the bins are defined such that they contain a defined fraction of the overall data set (for the case depicted in Figure 8, we selected four bins with 15/35/35/15% of the collection area). In addition, only intervals are selected, where the stellar limiting magnitude was better than magnitude 1.5, because otherwise there are too few stars for a reliable limiting magnitude estimate. Data-driven binning ensures that all graphs contain a sufficient number of meteors, and in our SPE example, the intersection point becomes indeed more accurate (Figure 8).

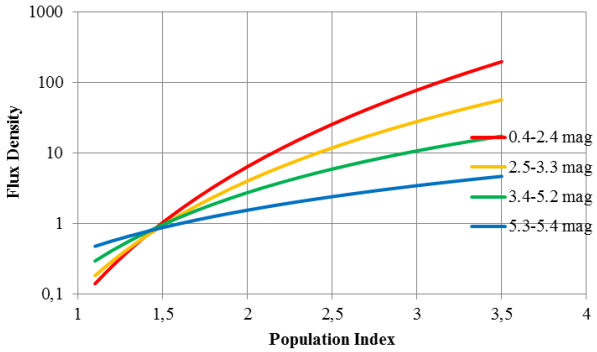

Figure 8 – Same plot as Figure 7, but the bins in meteor limiting magnitude are now defined is a data-driven way to ensure that each graph contains a sufficient amount of data.

The problem of the discrimination of the individual *lm* classes is addressed by applying a Poisson distribution.

Short reminder: Given random, independent events with a constant average rate λ per time unit, the (discrete) Poisson distribution $P_\lambda(k)$ provides the probability, that in a particular time unit exactly k events occur.

A practical example: Let's assume that sporadic meteors occur at an average rate λ equal to 5 per hour. The Poisson distribution will tell us the chance that in any particular hour, we observe 0, 1, 2, 3 … sporadic meteors (Figure 9). Obviously, the probability to observe 4 or 5 meteors is highest, but the chance that 10 meteors are observed is also not negligible.

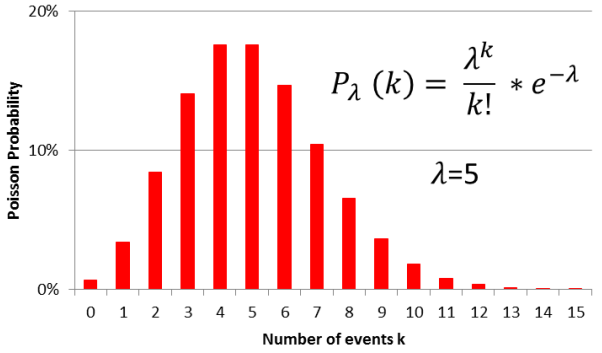

Figure 9 – Example for a Poisson distribution. The bars give the probability that 0 to 15 event are observed per time unit (e.g. sporadic meteors per hour), when the average rate λ is 5 events per time unit.

Now how is the Poisson distribution applied to our population index calculation? Starting from the overall

collection area over all limiting magnitude bins, we can calculate which fraction belongs to which limiting magnitude class. This fraction depends on the population index: For low *r*-values, the contribution of wide-angle cameras with low limiting magnitude will be higher (they are more efficient when many bright meteors are present), whereas for large *r*-values the cameras with smaller field of view and better *lm* become more effective. The meteor count is directly proportional to the collection area, so given the overall number of meteors recorded in a certain time interval we can calculate, how many meteors are expected in which limiting magnitude class (solid lines in Figure 10). Note that this figure will vary largely for cameras at the upper and lower end of the limiting magnitude spectrum, but that the expected meteor count varies only little for the intermediate cameras. They contribute only little information to the population index calculation.

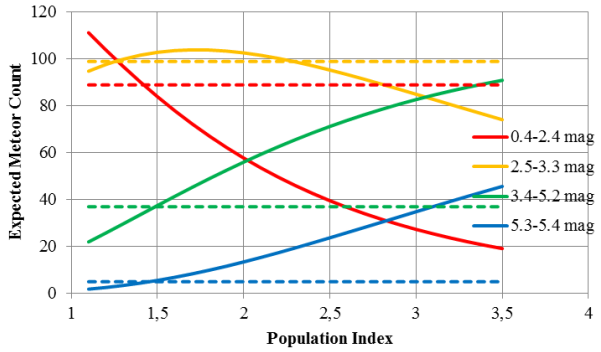

Figure 10 – The same data set as in Figure 8 in a different representation. Solid lines mark the number of expected meteors per limiting magnitude class, dashed horizontal lines the actually observed number of meteors.

Also given in Figure 10 is the actually observed number of meteors in each limiting magnitude class (horizontal lines). The best population index is the one where the observation and the expectation values are identical, but again there is not a single *r*-value were all pairs of graphs intersect.

This is where the Poisson distribution is applied: for each graph and each population index, it tells us the probability for the observed number of meteors *k*, given the expected number of meteors λ. In Figure 11, we print those Poisson probabilities for the four limiting magnitude classes, and the combined probability. They are represented as log probabilities and normalized by their maximum value, i.e. that the log peak probability of each graph is zero. The maximum of the combined probability graph yields the best population index.

Applying the Poisson distribution has two advantages:

- The number of meteors belonging to each *lm* class is taken into consideration, because the Poisson distribution is different for small and large values of λ and *k*.
- Graphs which are not discriminative for the determination of *r* contribute only marginally to the optimization (the Poisson distribution has a wide peak for these).

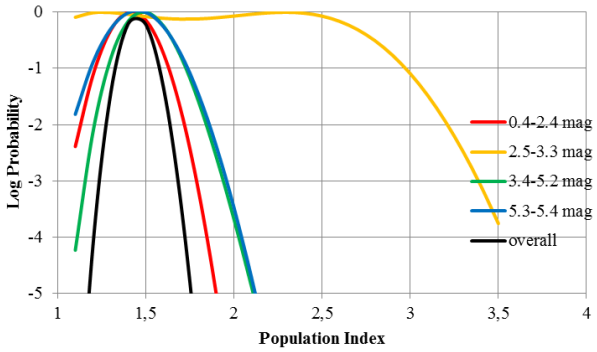

Figure 11 – Poisson (log) probabilities for the individual limiting magnitude classes in the previous figure normalized such that the maximum is always zero. Note that the second *lm* class provides only little information about the population index, because the expected meteor count depends only little on the population index. So this graph contributes only little to the overall probability.

Looking at a wider scale, the whole new procedure to calculate population indexes has some unique characteristics:

- It is independent of the meteor brightness, which is hard to determine reliably from video observations of meteors.
- It is resistant to possible systematic errors in the stellar limiting magnitude calculation. Since all limiting magnitude classes are affected in the same way, such an error will shift all graphs in Figure 8 vertically by the same amount, but not horizontally. That is, only the flux density will be affected, but not the *r*-value.
- For the same reason, the procedure is also immune to systematic errors on the meteor detection probability depending on the limiting magnitude. Again, all limiting magnitude bins are affected in the same manner which impacts the flux density, but not the population index.
- Some experiments have shown that the zenith exponent has also just a little impact on the calculation of the population index.

In practice, the combined Poisson probability over all limiting magnitude classes is calculated for selected *r*-values, and then a quadratic function $ux^2 + vx + w$ is fitted to the peak *lm* bin and the two neighbors. This five-point-fit matches closely the combined probability distribution. By simple differentiation of the quadratic function, we get a closed form solution for the best population index $r = v/2u$. Furthermore, the absolute value and the width of the combined probability graph give an indication for the error bars of the population index estimate.

5 Preliminary Results

During the development of the new approach in 2013/2014, it was tested on different meteor showers. Figure 12 gives an overview of *r*-values obtained for the September Perseids and Orionids in 2013, as well as the Quadrantids and Lyrids in 2014. A wide range of population indexes between 1.4 and 2.3 is obtained for the peak times of these meteor showers, and in most cases the intersection point is well-defined. However, that is not always the case for other dates and meteor showers.

For obvious reasons, the ultimate goal is not to obtain single *r*-values for meteor shower peaks, but whole population index profiles over the full activity period of a meteor shower. For this purpose, two programs are currently developed that implement the new approach. One is a fat-client application by S. Crivello running on Win XP, and the other an extension of the flux viewer web service by G. Barentsen (Barentsen and Molau, 2013)[1]. Both are still under reconstruction, so we can present here only some preliminary graphs for different major meteor showers in 2011 till 2013 (Figure 13). Even though the approach is new, we can still use all IMO Network observations where flux and limiting magnitude data are available (i.e. starting from spring 2011), since the new power function exponent *b* can be calculated afterwards from these data. The recalculation was computationally demanding (1 CPU month), but it is finished meanwhile. So after a phase where the optimal settings for the approach are determined (outlier rejection criteria for cameras with poor *lm* calculation, number of limiting magnitude classes and their share from the overall collection area, etc.) we expect more accurate population index profiles in the near future.

6 Discussion

The first results are promising and yield population indexes similar to those obtained from visual observations. Still, our *r*-values are typically somewhat smaller than the visual results. A detailed comparison between visual and video data revealed the following differences:

- In case of video observations, we use the absolute meteor magnitude *M* (i.e. normalized to 100 km altitude), whereas in visual observations the apparent magnitude *m* is used.
- The observing direction (altitude, radiant distance) is properly accounted for only in case of video observations.
- The effect of meteor motion on the limiting magnitude (fast meteors distribute their photons over more pixels) is only accounted for in case of video observations.

These differences may be the root cause for the observed differences.

7 Summary

After presenting why the population index is particularly important for flux density measurements from video meteor observations, we have shown that the traditional procedures for population index calculation do not fit well. For this reason, we derived and refined step by step a new approach that is specifically helpful if a large variety of video cameras with different limiting magnitudes is available. We have shown that the new approach provides certain desirable properties, and first population index profiles obtained from the IMO Network video observations look promising.

Acknowledgements

We are in great debt to all observers of the IMO Video Meteor Network, who collected over years a unique database of video meteors. The Video Meteor Database of IMO is a treasure that allows a wide range of new analysis techniques and results, for which the one presented here is a practical example.

References

Arlt R. (2003). "Bulletin 19 of the International Leonid Watch: Population index study of the 2002 Leonid meteors". *WGN, Journal of the IMO*, **31**, 77–88.

Barentsen G. and Molau S. (2013). "Meteoroid stream flux profiles derived from the IMO Video Meteor Network". Poster at Meteoroids 2013 Conference, A. M. University, Poznań, Poland, 26–30 August 2013. Not published.

Molau S., Barentsen G. (2013). "Status and history of the IMO Video Meteor Network". In Jopek T. J., Rietmeijer F. J. M., Watanabe J., and Williams I. P., editors, *Meteoroids 2013, Proceedings of the Astronomical Conference*, held at A. M. University, Poznań, Poland, 26–30 August 2013, A.M. University Press, 297–305.

Rendtel J. (2013). "From Rates to Fluxes of Meteoroid Streams". In Gyssens M., Roggemans P., and Żołądek P., editors, *Proceedings of the International Meteor Conference*, Poznań, Poland, 22–25 August 2013, IMO, 121–125.

Rendtel J., Lyytinen E., Molau S., Barentsen G. (2014). "Peculiar activity of the September epsilon-Perseids on 2013 September 9". *WGN, Journal of the IMO*, **42**, 40–47.

[1] http://www.imonet.org/imc13/meteoroids2013_poster.pdf

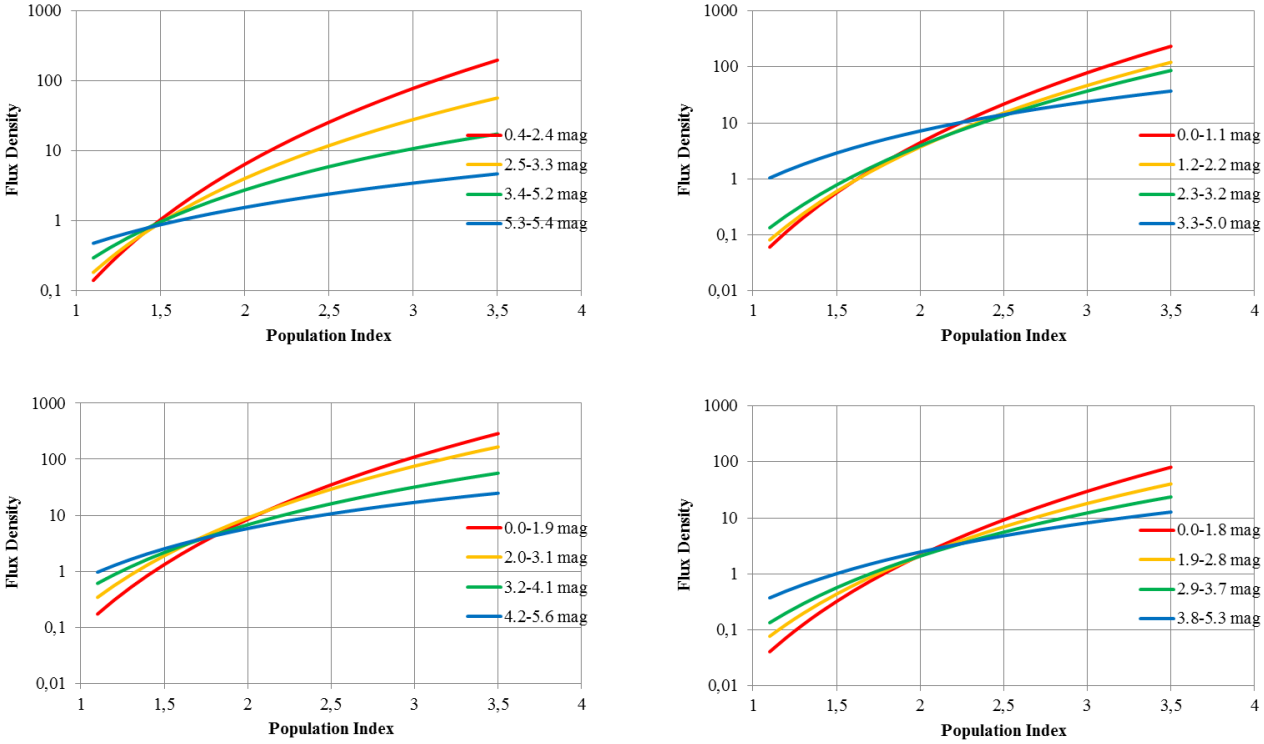

Figure 12 – Population indexes obtained for individual meteor showers near their peak times: *September Perseids* on Sep 9/10, 2013, (top left); *Orionids* on Oct 23/24, 2013, (top right); *Quadrantids* on Jan 3/4,2014, (bottom left); *Lyrids* on Apr 22/23, 2014, (bottom right).

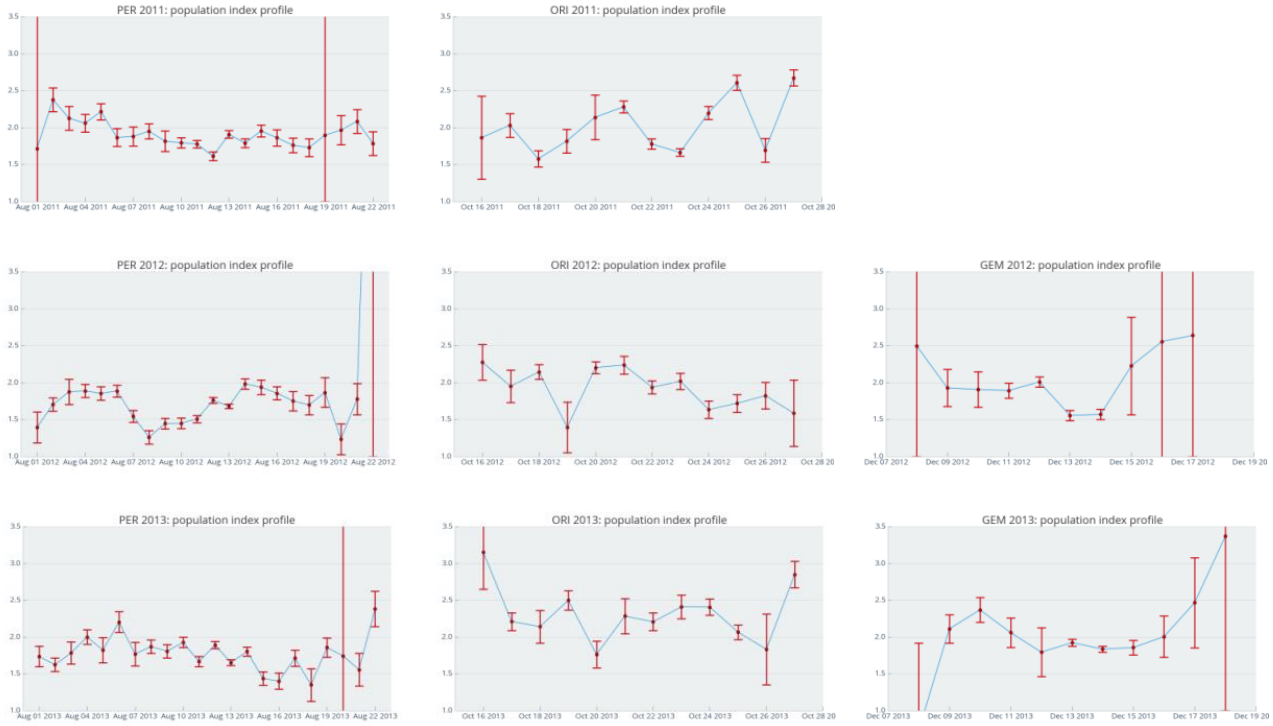

Figure 13 – First preliminary population index profiles for the *Perseids* (left), *Orionids* (center) and *Geminids* (right) in 2011 (top), 2012 (center) and 2013 (bottom).